XLab Frascati: Beams Channeling for Basic and Applied Studies

S.B. Dabagov (Resp.), D. Hampai, V. Guglielmotti (Ass.)

Collaborations:

Italy:	INFN - Laboratori Nazionali di Frascati
	INFN - Milano Bicocca
	Dip. DAFNE, Universitá degli Studi della Tuscia, Viterbo
	Dip. Scienze e Tecnologie Chimiche, Universitá Tor Vergata, Roma
	Dip. Scienze dell'Antichitá , Universitá Sapienza, Roma
	Dip. Scienze Ingegneristiche, Universitá Guglielmo Marconi, Roma
	Dip. Ingegneria Civile, Universitá Niccolò Cusano, Roma
Russia:	RAS P.N. Lebedev Physical Institute, Moscow
	NR Nuclear University MEPhI, Moscow
	NR Tomsk Polytechnic University, Tomsk
	Southern Federal University, Rostov-on-Don
Switzerland:	CERN - European Organization for Nuclear Research
USA:	Fermilab - Fermi National Accelerator Laboratory

The XLab Frascati (XlabF) laboratory is a unique Italian laboratory aimed generally in the research of beams channeling in various media related to both theoretical and experimental studies, which, in its technological part, is dedicated to the design, manufacture and characterisation of X-ray/neutron polycapillary optics (polyCO). Involved in several national and international projects and collaborations, XlabF is focused on theoretical investigations of (a) the dynamics of charged and neutral channeled beams in crystals and other micro- and nanoguides (crystals, capillaries, microchannel plates, etc.), and (b) the electromagnetic radiations emitted by charged particles in various ordered solid structures, as well as (c) on the application of polycapillary optics for X-ray analysis in various fields, such as cultural heritage, innovative materials, medical diagnostics, pharmacology, beam diagnostics, detectors characterisation, etc. The laboratory experimental activities aim in particular in both characterising novel optics and evaluating various practical schemes for different X-ray applications such as X-ray diffraction (XRD), X-ray fluorescence (XRF and TXRF – total reflection X-ray fluorescence) and X-ray imaging. XlabF technological studies result in the design and development of various instrumental prototypes and new X-ray desktop facilities for advanced analytical techniques as well.

1 Facilities @ XlabF

Presently, at the XlabF facility, three stations (RXR, XENA, PXRDS) are open to users: their combined work allows various analysis to be optimised and matched, while two more stations are actually on the stages of realisation and commissioning (CTS and Soft-XRF).

1. XENA (*X-ray Experimental station for Non-destructive Analysis*) is operative. It is equipped with three X-ray Oxford Apogee tubes (W, Mo and Cu anodes), a set of mechanical components and motors for lens alignment and scanning, and an optical table providing many

geometrical setup possibilities. At the beginning, being the unique experimental station, it was used for all the different X-ray analysis performed at the laboratory. Today, XENA is a facility dedicated exclusively to imaging, tomography and characterisation of X-ray devices such as novel sources, optics - diffractive crystals and vibrating optics - and detectors.

2. RXR (*Rainbow X-ray*) is an optimised system of XENA for 2D/3D XRF micro-imaging and TXRF. It is equipped with two detectors of different energy efficiency, in order to measure a full spectrum ranging from 800 eV to 25 keV. RXR works in confocal mode: the source is coupled with a full-lens, and both the detectors are combined with dedicated half-lenses. RXR is also equipped with an optional vacuum chamber for measurements in the low energies range. This vacuum chamber has the possibility of inserting a polyCO for TXRF analysis.

3. PXRDS (*X-ray Diffractometer Station*) is a $\Theta/2\Theta$ "Seifert - XRD 3003" diffractometer. The instrument has a remarkable mechanical stability, high precision and a variety of possible configurations. The diffractometer is a 2200W Power System with a Cu$K\alpha$ anode target, 1x12 mm beam, while the goniometer, placed in a vertical position, has a high precision thanks to the use of stepper motors with micro-step movement which ensures an angular resolution greater than $0.001°$.

4. CTS (*Computed Tomography Station*) is a measuring station for high precision tomography. Developed as part of a *Premiale* project, the station, equipped with a micro-focusing source (4 μm on the anode), high precision mechanics and high-resolution CCD detector (10.4 μm per pixel), through the phase retrieval technique CTS can reach a resolution estimated about 600-700 nm per voxel. CTS is currently in the installation and commissioning phase.

5. SoX (*Soft-XRF*) is the new fluorescence station for the study of organic materials. The main characteristics of this instrument is the high vacuum chamber, the 6-axis manipulator for positioning and a windowless detector necessary for detection of low atomic number elements, such as Carbon, Oxygen, Nitrogen and Fluorine. Actually we are implementing the station, with a dedicated detector for low energies.

2 Activity in 2021

2.1 Volume Photography

During 2021, the XlabF team was involved in several projets. Actually, thanks to the collaboration with both G. Marconi and Tor Vergata Universities, we have carried different studies based on the use of X-ray spectroscopies such as elemental analysis by microXRF to estimate the presence of specific chemical components and structural studies by XRD to confirm the morphology of the material under examination.

In particular we studied: a) inorganic materials in collaboration with UniMarconi (i.e. nanostructured oxides) to be used as element of SOFC (solid oxide fuel cell) for industrial systems adopted for production of syngas starting from biomass (BLAZE European Project), b) both by microXRF and PXRD, the composition of inorganic compounds used as luminescent material for photon radiation dosimetry in collaboration with Tor Vergata University (Prof. G. Paradossi), c) the composition of pigments within some ancient artefacts (an ancient book and two Buddhist scrolls) in collaboration with Tor Vergata University and the museums/collections to which the samples belong by using microXRF aiming at mapping specifically some points of the sample, d) several specimens (from inorganic like parts of ancient buildings to organic ones) coming from the Peltuinum excavation site (located in Abruzzo near L'Aquila) in collaboration with Prof. L.

Migliorati (Sapienza University) to evaluate the kind of material both in terms of crystalline structure (by XRD) and as chemical species present (by XRF) aiming in supporting the archeologists in their studies based on the information gained during the years on the excavation site.

@ *CTS - Status.* The mechanics of the station for micro tomography (CTS) have been realised, respecting the safety requirements for X-rays up to 100 keV, Fig. 1, a.

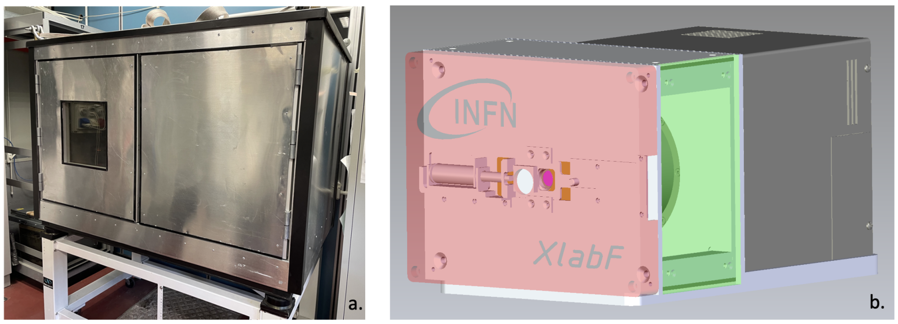

Figure 1: *a. CTS experimental setup. b. Mechanical design of the CTS Shutter.*

The Pb protective layer with a thickness of 3 mm completely envelops the experimental hutch, while the surface of the side opposite to the source is covered with Pb of 6 mm of thickness. A system of microswitches allows the use of the facility in a complete safety mode by acting directly on a shutter entirely designed and realised in collaboration with the services of Officina Meccanica of LNF, Fig. 1, b.

The electronics, relating to movements, power supply source and safety devices, is in the commissioning phase (in collaboration with Servizio di elettronica - Automazione e Controllo di LNF) and the starting phase of the CTS in the operative mode is expected in March 2022, in collaboration with the Fisica Sanitaria group. We foresee to analyse first organic samples, to test the performance of the facility, in April-May 2022.

@ *XRF Analysis Tool.* A qualitative and semi-quantitative Fluorescence analysis software was developed at XlabF, both for point studies and for 2D and 3D mapping measurements. The software is based on LabVIEW platform and allows to:

1. evaluate and recognise the elements present in a spectrum (qualitative analysis);

2. carry out advanced fitting analysis by the deconvolution of the spectrum and convolution of single elements peaks, Fig. 2;

3. evaluate relative concentrations of the chemical species using the Fundamental Parameters Method (FPM) in the approximation mode of very thin samples;

4. reconstruct two-dimensional (2D) and three-dimensional (3D or Color-CT) maps of chemical elements analsyzed, Fig. 3.

@ *Cultural Heritage Samples.* In collaboration with Universitá di Roma "Tor Vergata", the Casanatense Library (for Manuscript 92), the Ragusa Foundation and the Pigorini Museum (emakimono 142 838 and painted roll n.142 846), we studied the ink present in few ancient artefacts. The objective of the work was the determination of chemical components of the inks present within several areas of two different sample typologies (an ancient manuscript and some Buddhist scrolls), Fig. 4.

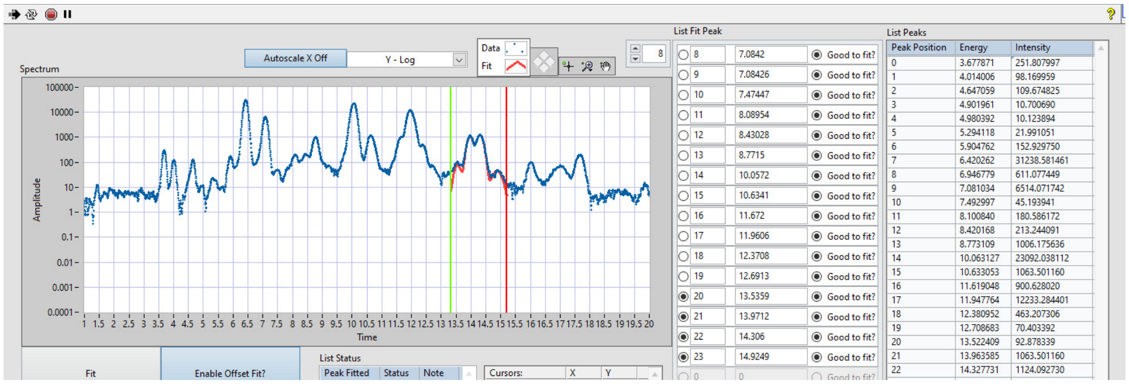

Figure 2: *Example of multi-fit analysis for 4 peaks.*

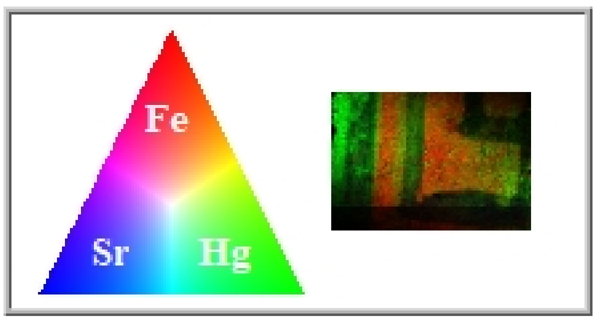

Figure 3: *2D μXRF reconstruction.*

We aimed to the extraction of semi-quantitative results following a methodology that was primarily tested on an XRF standard, apart from the qualitative recognition of the elements constituting the inks. Reporting the experimental results achieved on both the artefacts, we have studied the XRF emissions, obtaining element concentration (in %), that has led us to confirm the hypotheses coming from the bibliographic history of the artefacts, in order to fine-tune the further restoration procedure.

The results obtained by applying the FPM (Fundamental Parameter Method) approach during the studies on the Buddhist scrolls for the estimation of relative concentrations for the chemical elements responsible of the target pigments lead to the preparation and publication of a scientific paper on the RPC journal firstly, and later on the experimental results achieved from this study were exposed at the AIC2021 Conference (by the Tor Vergata team) gaining further success (a proceeding was published as follow up) and leading to a second publication on the journal SCIRES-IT(http://www.sciresit.it/), within a special edition issue as best paper selected among those presented at the conference. The paper was submitted recently and it is under revision.

@ *Forestry Sciences Samples.* In collaboration with Universitá of Viterbo Tuscia, we still continued to analyze tree samples from UNESCO sites for the evaluation of the presence of atmospheric pollutants (Pb, Cu and other heavy metals) and the study of the biology of these trees.

@ *Antarctic and Alpine Ice Core Studies.* Milano Bicocca, in collaboration with several Universities and Research Institutes, following the studies at the SSRL and Diamond Synchrotron Laboratories and at the XLab Frascati Laboratory, has published a summary work on Nature regarding the analysis on insoluble particles extracted from ice core campaigns at the Antarctic sites (Talos Dome and Epica) and at the alpine site of Colle del Lys [1].

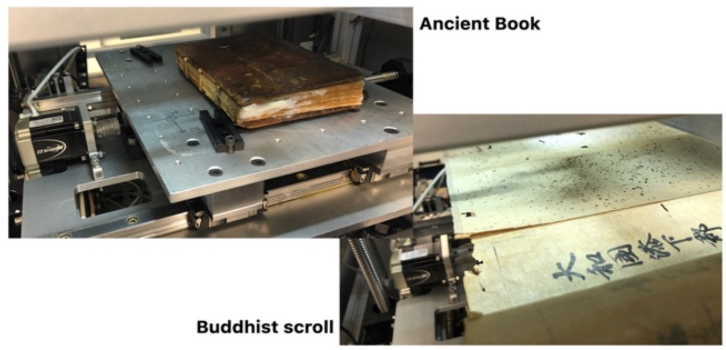

Figure 4: *Pictures of two artefacts studied by XRF Spectroscopy housed in the RXR facility: The Ancient Book (up left picture) and the Buddhist scroll (bottom right picture).*

Preliminary studies of Fluorescence were carried out at the XlabF both in normal incidence and in grazing incidence, useful for defining a measurement protocol for a Conventional Laboratory in order to be more efficient in the analysis of future Antarctic cores [4].

2.2 Fermilab Muon g-2

In April 2021 the first results of the Fermilab National Accelerator Laboratory (FNAL) Muon g-2 Experiment for the positive muon magnetic anomaly $a_\mu \equiv (g_\mu - 2)/2$ have been announced [6–9]. The anomaly is determined from the precision measurements of two angular frequencies. Intensity variation of high-energy positrons from muon decays directly encodes the difference frequency ω_a between the spin-precession and cyclotron frequencies for polarised muons in a magnetic storage ring. The storage ring magnetic field is measured using nuclear magnetic resonance probes calibrated in terms of the equivalent proton spin precession frequency $\tilde{\omega}'_p$ in a spherical water sample at 34.7 °C. The ratio $\omega_a/\tilde{\omega}'_p$, together with known fundamental constants, determines $a_\mu(FNAL) = 116592040(54) \times 10^{-11}$ (0.46 ppm). The result is 3.3 standard deviations greater than the standard model prediction and is in excellent agreement with the previous Brookhaven National Laboratory (BNL) E821 measurement. After combination with previous measurements of both μ^+ and μ^- , the new experimental average of $a_\mu(Exp) = 116592061(41) \times 10^{-11}$ (0.35 ppm) increases the tension between experiment and theory to 4.2 standard deviations (Fig. 5).

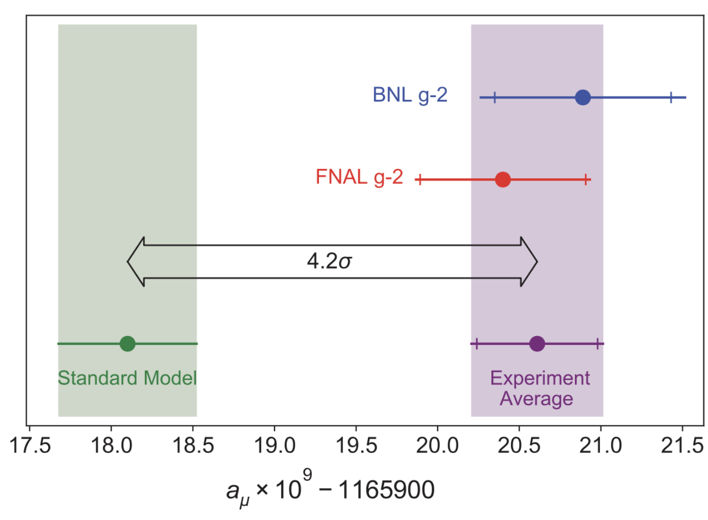

Figure 5: *From top to bottom: experimental values of a_μ from BNL E821, Fermilab measurement, and the combined average. The inner tick marks indicate the statistical contribution to the total uncertainties. The Muon g-2 Theory Initiative recommended value for the standard model is also shown [7].*

2.3 Channeling Related Studies

@ Channeling Radiation at Axial Channeling in Crystals. Channeling of light relativistic particles in crystals is accompanied by intense radiation emission known as channeling radiation (CR). Typically all calculations of channeling radiation aim in getting the total radiation intensity and its dependence on the parameters of particles and crystals. In the same time, since the discovery, the angular behaviours of channeling radiation have been studied just in a few works, in which only a polar dependence of the radiation intensity near the forward direction is estimated. However, simple analysis of the interaction potential predicts very specific features to be observed in the angular distributions of channeling radiation, especially at axial regime. In this work, for the first time, the expressions for angular and spectral distributions of electromagnetic radiation at axial channeling of relativistic charged particles in thin crystals are analytically refined within the QED theory [11]. Obtained results allows predicting complex structures of radiation intensity and polarisation distributions (Fig. 6). The results obtained might be of special interests for experimental studies.

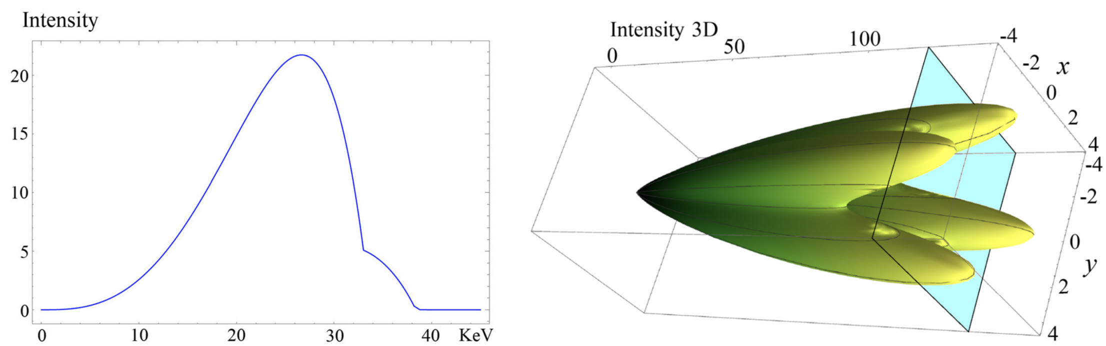

Figure 6: *left: CR spectral distribution for 10 MeV electrons axially channeled in Si ⟨100⟩ (the intensity is given in arbitrary units). right: CR angular distribution for 10 MeV electrons channeled in Si ⟨100⟩ crystal (the arbitrary units have been used).*

Evaluating the possibility of observing the features of the angular distribution of channeled radiation calculated by us, it should be noted that it is usually believed that for low- energy particles the angular distributions of radiation will be quickly smeared by above-barrier particles arising due to incoherent scattering. An estimate of the dechanneling length for 10 MeV electrons at axial channeling in Si ⟨100⟩ gives the value $L_d = 0.215\,\mu m$. Obviously, this is rather short distance for 10 MeV electrons. However, during the time of flight of even this distance, electrons in any case generate CR, which can be registered experimentally; the emission of dechanneled electrons in the direction of the channeling axes is essentially suppressed. The intensity of CR can be increased if to use the electrons of higher energies, which are characterised by larger dechanneling length; for instance, we get $L_d = 1.1\,\mu m$ for 50 MeV electrons channeled in Si ⟨100⟩. As seen, even for a bit higher electron energy we deal with very thin crystals ($\sim 1\mu m$) that proves the feasibility of recording the picture similar of one presented in Fig. 6. Reported calculations based on the newly deduced formulas for the radiation intensity show that the CR angular distributions have a much more complex structure in com- parison with the results obtained in the approximation of a single crystal axes. This structure is associated with the crystal symmetry in general and in the transverse plane as well. So, for example, for a Si ⟨100⟩ crystal, four peaks should be observed in the angular distributions, located symmetrically about the crystal axis. The CR angular distribution geometry uniquely demonstrates an explicit dependence of the CR probability on the azimuthal angle.

@ *Channeling of Synchrotron Radiation in MCP Systems.* Synchrotron radiation sources have been used to study the focusing properties and angular distribution of X-ray radiation at the exit of spherically bent microchannel plates (MCPs) [16]. In this contribution it is shown how soft X-ray radiation at energies up to 1.5 keV can be focused by spherically bent MCPs with curvature radii R of 30 mm and 50 mm (Fig. 7). For these devices, a focus spot is detectable at a distance between the detector and the MCP of less than R/2, with a maximum focusing efficiency up to 23% of the flux illuminating the MCP. The soft X-ray radiation collected at the exit of microchannels of spherically bent MCPs are analysed in the framework of a wave approximation. A theoretical model for the wave propagation of radiation through MCPs has been successfully introduced to explain the experimental results. Experimental data and simulations of propagating radiation represent a clear confirmation of the wave channeling phenomenon for the radiation in spherically bent MCPs.

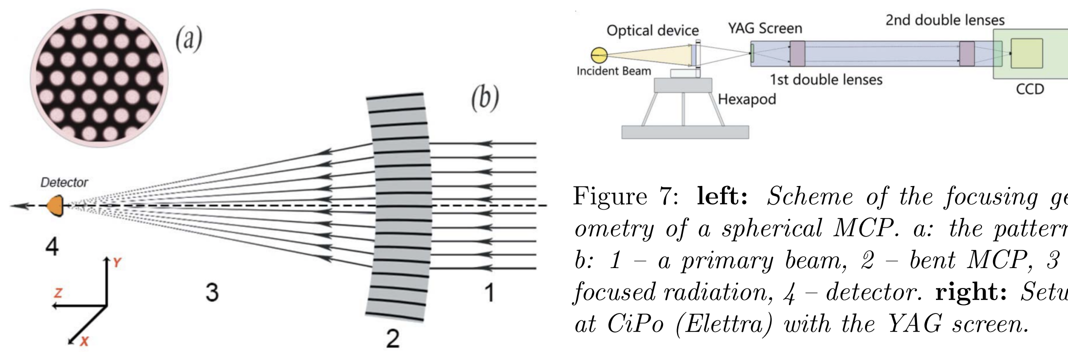

Figure 7: **left:** *Scheme of the focusing geometry of a spherical MCP. a: the pattern; b: 1 – a primary beam, 2 – bent MCP, 3 – focused radiation, 4 – detector.* **right:** *Setup at CiPo (Elettra) with the YAG screen.*

MCPs behave as efficient radiation waveguides in transmission. However, these diffractive optics may increase the flux density and focus X-ray radiation offering interesting perspectives for X-ray applications with high brilliant and highly coherent SR sources. In this study, we demonstrated the focusing properties of spherically bent MCPs with different curvature radius using two different synchrotron radiation sources (BESSY and Elettra) over a wide range of energy from 450 to 1500 eV (see, for instance, Fig. 8). To describe the obtained experimental results, not compatible with simple geometrical optical considerations, we applied a model based on the wave propagation of multiply scattered wavefronts. The simulation results of the MCP focusing are in excellent agreement in the energy range 450–1500 eV . We also measured the X-ray radiation distribution at the exit of spherically bent MCPs along the optical axis. These maps show that the focal distance between the detector and bent MCPs depends on the curvature radius R, and it is always smaller than the geometrical optical value of R/2. The result is supported by simulations and by experimental data collected with spherically bent MCPs at energies of 1000 eV and 1500 eV, i.e. when a small spot is achieved in correspondence to the highest transmitted intensity.

We have experimentally and theoretically characterised silicon-glass MCP devices doped with cobalt atoms. Under anomalous scattering condition near the SiL-edges and CoK-edge we have proved the coherent excitation and the axial propagation of the induced fluorescence radiation inside micro-channels [15]. Chemical modification of the MCP inner surface shows the efficient transmission of hard X-ray secondary radiation at the primary radiation energies of 100 eV and 8 keV. Experimental tests for these X-ray waveguides have been performed utilising both synchrotron radiation and conventional X-ray sources. X-ray pattern simulations point out that the propagating radiation has a waveguide modal character, which is described as axial channeling of the secondary fluorescence radiation.

The diffraction of X-rays at the output of a microchannel plate at the grazing incidence of

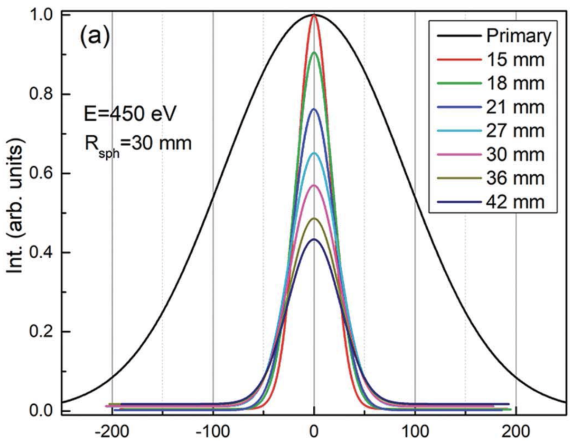

Figure 8: *Comparison of profiles and spot sizes (FWHM) of radiation collected by MCPs with two different radii of curvature at 450 eV (Elettra). All profiles have been normalised to the incident photon flux.*

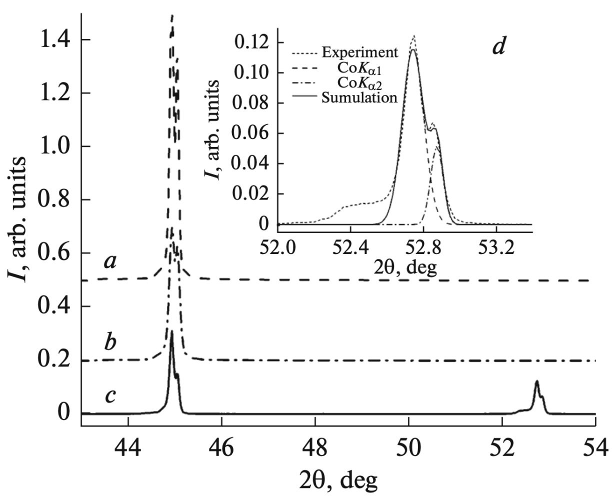

Figure 9: *Comparison of normalised X-ray diffraction patterns collected with the diffractometer. a: without the MCP; b: with a reference MCP; c: with the Co doped MCP; inset d: the two $CoK_{\alpha1,2}$ diffraction contributions.*

monochromatic radiation on the walls of microchannels has been studied both experimentally and theoretically (Fig. 9). The angular distributions of the radiation intensity at the output of polycapillary structures have been obtained by simulating the processes of excitation and propagation of X-ray fluorescence in hollow glass waveguides. The results are in agreement with experimental data. It has been shown that coherently excited SiL fluorescence propagates primarily in a direction close to the axis of microchannels. Consequently, most of the energy of secondary radiation can be transferred in this direction.

We have improved our theoretical model to calculate the focal spot properties of coherent SR soft X-ray beams by combining and aligning two MCPs (Fig. 10, left). The diffraction patterns of the radiation behind the MCP system have been simulated in the framework of the electrodynamical model of the radiation emission from two-dimensional finite antenna arrays. Simulations show that this particular optical device focuses the soft X-ray radiation in a circular central spot with a radius of $\sim 4\,\mu$m (Fig. 10, right). The study points out that such MCP-based devices may achieve micrometer and sub-micrometer spot sizes as required by many applications in the soft X-ray range. Finally, based on experimental and theoretical results of the radiation transmission by this MCP-based device, a new method to spatial properties of brilliant SR sources is discussed [11].

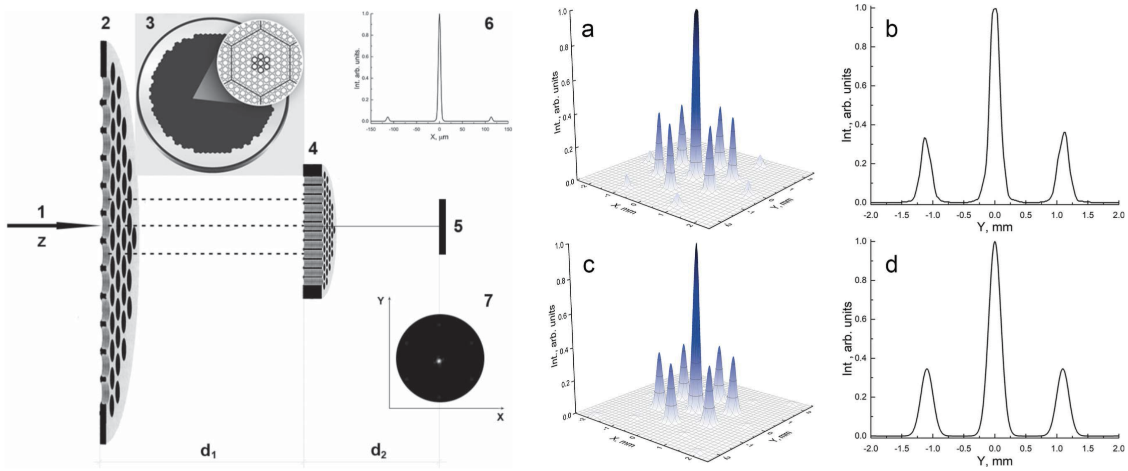

Figure 10: **left:** *Scheme of two flat parallel coaxial MCPs for focusing of the X-ray beam;* d_1 *is the distance between the two MCPs and* d_2 *the distance between the detector and second MCP. 1 – primary radiation; 2 – first MCP; 3 (inset) – image of the capillary structure of both MCPs; 4 – second MCP; 5 – 2D detector of radiation; 6 (insert) – focal spot profile; 7 (insert) – focal spot cross-section.* **right:** *MCP diffraction pattern and beam profiles in the selected plane at 94 eV. a, b - experimental data; c, d - simulated distributions.*

In the simulations of the MAAS (Microchannel Aligned Assembled System) device (Fig. 10, left), microchannel diameters as well as pitch sizes and periods may change to set the optimal parameters for focusing, interference, diffraction, etc. The model considers two MCPs of ideal hexagonal symmetry in the transverse cross-sections and with the symmetry axis along the z-axis. In the simulations, each MCP is characterised by its dispersion equation, optimised by suitable microchannels. The first MCP is used to shape the primary parallel beam (coherent or partially coherent). Behind the first MCP the beam becomes conical in shape, and this 'secondary beam' defines the radiation footprint on the surface of the second MCP, chosen thicker and with smaller microchannels.

The analysis of the radiation distribution at its exit highlights the possibility to control macroscopic properties of the parallel or quasi-parallel primary beam. Moreover, using the theoretical model we introduced, the analysis of patterns generated by properly aligned couples of MCPs could be used to evaluate the coherent fraction of a SR source or a FEL.

@ Features of Beams Guiding in a Capillary. Our recent studies allowed us revealing similar features for transmission of radiations and beams by capillary guides. The curvature of a capillary inner surface plays essential role in forming the reflecting potential for the quantum of either radiation or charged beam. Developed theory of the interaction between the projectile and surface subsystem based on the continuous surface potential formalism has demonstrated unique explanation for the efficient transmission of radiations and beams (see, for instance, in the cover picture of the Quantum Beam Science, vol. 6, issue 1 from March 2022, Fig. 11) [10,13].

Nowadays, the radiation waveguides are in a wide use to shape the electromagnetic radiation beams of a wide frequency range. This makes the radio and optical waveguides extremely attractive for various applications. Actually, X-ray waveguides are intensively in the research stage of development.

As is known, generally, the solution of Maxwell equations describing propagation of electro-

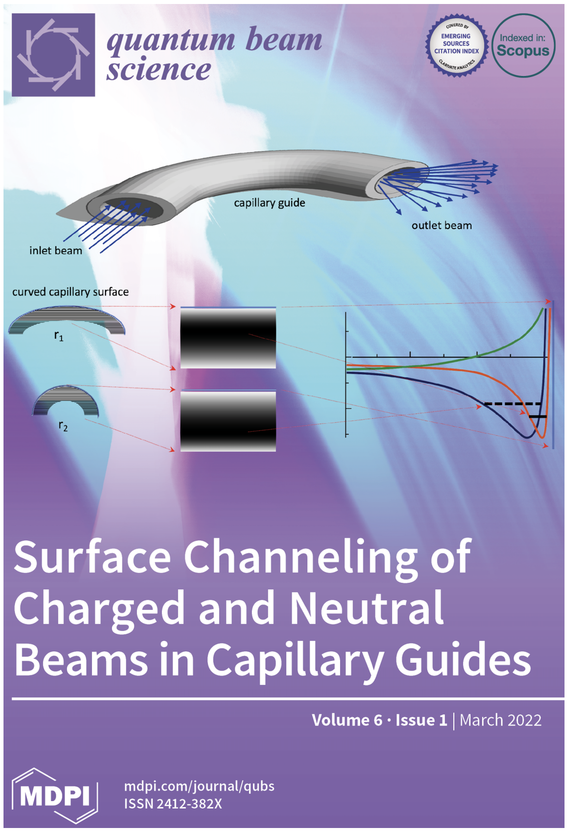

Figure 11: *The passage of charged and neutral beams through dielectric capillary guides can be described from a uniform point of view of beams channeling in capillaries revealing that the surface interaction potential for micro- and nano-capillaries is conditioned by the curvature of the reflecting surface. The effective beam guiding by a capillary is expressed from the general standpoint of quantum mechanics, which allows the interaction potential for surface channeling to be analytically explored. Depending on the projectile and channel-forming insulator characteristics, the interaction potential can be either repulsive or attractive that, as discovered, at fixed beam parameters manifests the ejection (expulsion) of both types of particles towards the center of the guiding channel at the decrease in the capillary diameter (from [10]).*

magnetic waves in media with a step-function index of refraction and results in forming a discrete set of the modes. Applied to capillary guides, our analysis of X-ray radiation propagation into the guides of various shapes shows that all the observed features can be described within the unified theory of X-ray channeling: surface channeling in μ-size guides and bulk channeling in n-size guides. The ratio between the transverse wavelength of radiation and the effective size of a guide, i.e., $\lambda_\perp/d \equiv \theta_d/\theta_c$, in other words, the ratio between the diffraction and Fresnel angles, herein determines the main criterion defining character of radiation propagation. If this ratio is small, the ray optics approximation is valid, and we deal with the large number of bound states. In turn, at $\lambda_\perp \simeq d$, a few modes will be formed in a quantum well of the interaction potential, along with just a single mode, for $\lambda_\perp \gg d$. Solution of the wave equation of the radiation propagation in such guides, moreover, demonstrates that at the center of a guide the flux peaking of x radiation, i.e., the increase of the channeling state intensity in the center of a guide, should take place. This feature is a proper channeling phenomenon and can be explained only by the modal regime of radiation propagation. The latter is of particular interest to researchers.

A similar problem of interaction of a charged particle with the inner surface of a cylindrical cavity in an infinite insulator has been also analysed based on the Hamiltonian formalism. We have succeeded in reducing the interaction potential for a charged particle in the field of surface excitations. Neglecting excitations of the wavelengths comparable to the cavity radius, the interaction potential has been explicitly written revealing its complex nature. An imaginary part of the potential leads to a finite width of the energy levels and is not examined in a general form. However, as an example, the energy losses of a particle per unit of traveled distance are obtained at its interaction with surface plasmons. The analysis of a real part of the potential, instead, has been carried out for two limiting cases.

We have shown for the first time that at the limit $\omega_s R_0/v \ll 1$, the induced potential of interaction of a charged particle with the cavity surface acts as a scattering potential (forming a reflecting barrier), while at $\omega_s R_0/v \gg 1$, it reveals a potential well near the surface (Fig. 12). The width of the potential well depends on the speed of the particle, i.e., the higher the speed of the particle, the wider the well. In both cases considered, the real potential logarithmically tends to plus infinity. The maximum value of the induced potential mainly depends on the particle charge and its longitudinal velocity. The estimates performed show that the averaged atomic potential is much higher than that induced for one particle, while for a beam of many particles channeled in a capillary, the maximum value of the induced potential is expected to be essentially different.

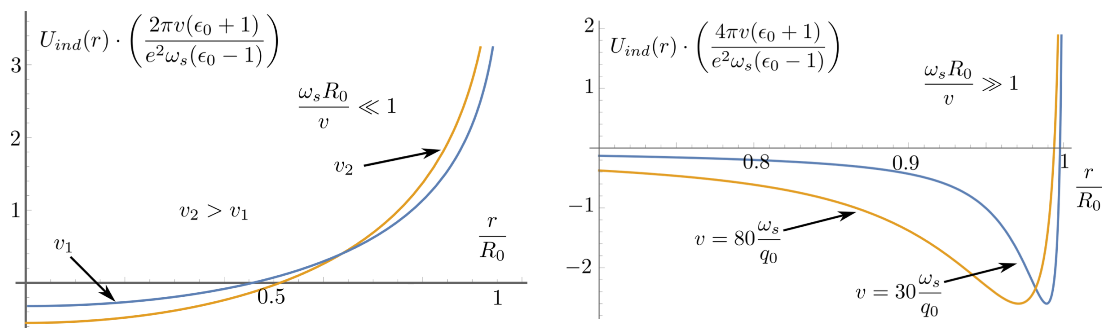

Figure 12: *Dimensionless induced potential versus the distance from the cavity axis at the condition* $\omega_s R_0/v \ll 1$ **(left)**, *while a concrete plotting is for* $q_0 R_0 = 10^3$ *and* $\omega_s = 10^{15}\,c^{-1}$, *with the characteristic value* $q_0 \sim 10^7\,c^{-1}$ *corresponding the cavity radius* $R_0 \sim 10^{-4}$ *cm, and at the condition* $\omega_s R_0/v \gg 1$ **(right)**. *Two curves correspond different values of longitudinal velocity. As can be seen, at the particle velocity increase the potential shape does not change, and the curve minimum tends to the cavity center.*

The theoretical results obtained for charged particles allow us to explain within unique approach (model) different features of charged particles transmission by capillaries of various diameters. These characteristics might be absolutely opposite to the results obtained if described within simple thermodynamic principles for particle diffusion models. The latter makes it necessary to use different models to describe the results of the same experiment. The proposed theory, in our opinion, will help to circumvent these difficulties. We hope that this work, in addition to known theories and models, will lead to a better understanding of the physics of surface channeling of charged particles along curved surfaces, will allow a better understanding of the process of effective transmission of particle beams by capillaries, and will contribute to the continuation of active research on the formation of charged particle beams by capillary structures.

2.4 Novel Compact Powerful Radiator

We have investigated the angular distribution of electromagnetic radiation by a chain of relativistic charged particles uniformly rotating along the equatorial orbit around a dielectric ball [14]. At a certain rotation frequency in combination with weak absorption of radiation in the ball, the radiation intensity becomes significantly higher than the corresponding value for a chain of charges rotating in a vacuum or in a transparent medium with the same dielectric constant as that of the ball's material. Having selected the parameters of the problem at which the charges in the chain emit coherently, we have shown that the radiation intensity at a given harmonic increases in proportion to the square of the number of emitting charges. The numerical results obtained for the different dielectric balls have revealed the emitted radiation to be in the GHz/THz frequency ranges. The powerful radiation of the chain propagates in the range of angles determined by the Cherenkov condition for the velocity of the chain projection onto the ball surface that is an additional factor, which must be taken into account to evaluate the radiation amplification (Fig. 13).

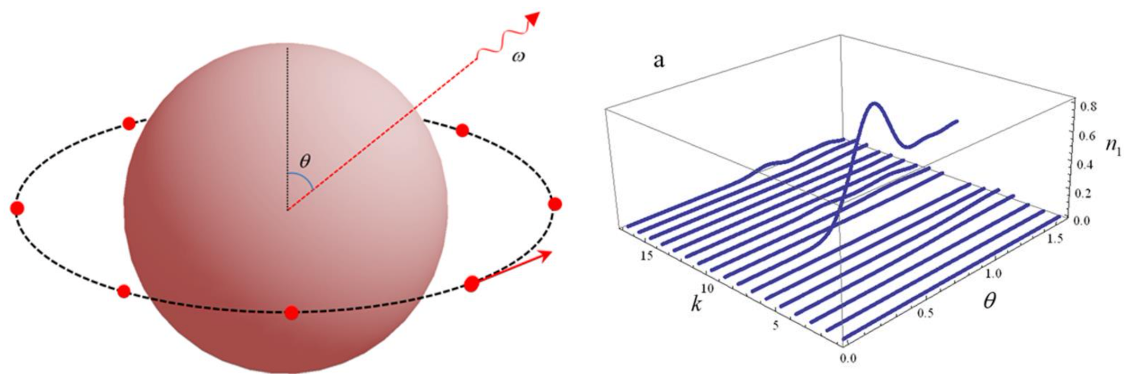

Figure 13: **left:** *A chain of relativistic electrons rotating around a ball in its equatorial plane.* **right:** *The angular distribution of radiation flux generated by one electron at one turn as a function of the harmonic number k. a – a rotation around the dielectric ball.*

We have demonstrated that an electron rotating uniformly around a dielectric ball, at certain values of the parameters of the system, can generate radiation at a given harmonic k_0, which is several tens of times more intense than the radiation generated by an electron rotating in a homogeneous medium having the same real part of the dielectric constant as the material of the ball. The powerful radiation is emitted due to the fact that the electromagnetic oscillations of the Cherenkov radiation generated by a particle inside the ball along its entire trajectory are partially locked inside the ball and, being repeatedly reflected, can overlap each other creating constructive interference.

3 List of Lectures & Talks by LNF Authors

1. G. Guglielmotti, *Advanced spectroscopy and microscopy studies for chemical elements evaluation by micro-X-ray Fluorescence and polycapillary optics*, High Precision X-ray Measurements, INFN-LNF, Frascati, 8-10 June 2021, Italy.
2. G. Guglielmotti, *Polycapillary X-ray techniques for archeological studies: the Peltuinum excavation site*, ISRP-15, Kuala Lumpur, 6-10 December 2021, Malaysia
3. D. Hampai, *Advanced X-ray Studies @ XlabF", High Precision X-ray Measurements*, INFN-LNF, Frascati, 8-10 June, 2021, Italy.
4. D. Hampai, *High Resolution CT @XlabF: Future Tomographic Studies*, ISRP-15, Kuala Lumpur, 6-10 December 2021, Malaysia.
5. S. Dabagov - invited lecture *Surface Channeling for Beams and Radiations Shaping*, 7th International conference Electron, Positron, Neutron and X-ray Scattering under External Influences, 18-23 October 2021, Yerevan, Armenia
6. S. Dabagov - invited talk *Channeling X-rays for Coherence Measurements*, HPXM - High precision X-ray measurements LNF conference, 8-10 June 2021, Frascati, Italy
7. S. Dabagov - invited lecture *Channeling in Optical Lattices*, South Federal University, 9 April 2021, Rostov-on-Donu, Russia
8. S. Dabagov - plenary lecture *Robert Avakyan: ... Channeling in Physics ...*, a memorial lecture at the Robert Avakyan's 90th anniversary meeting, 6 April 2021, Yerevan, Armenia

9. S. Dabagov - invited talk *X-ray Spectroscopy and Microscopy Studies at XLab Frascati*, 3rd International Forum on Advances in Radiation Physics (IFARP-3), 24-25 February 2021, Kuala Lumpur, Malaysia

References

1. G. Baccolo, B. Delmonte, P.B. Niles, G. Cibin, E. Di Stefano, D. Hampai, L. Keller, V. Maggi, A. Marcelli, J. Michalski, C. Snead, M. Frezzotti, Jarosite formation in deep Antarctic ice provides a window into acidic, water-limited weathering on Mars, *Nature Comunications* **12** (2021) 436.
2. G. Cappuccio, S.B. Dabagov, D. Hampai, C. Mazzuca, L. Micheli, M. Redi, PolyCO in XRF analysis: Fundamental Parameter Method Applied for Japanese Buddhist Scroll Studies, *Radiation Physics and Chemistry* **188** (2021) 109660 doi: 10.1016/.radphyschem.2021.109660
3. A. D'Andrea, L. Severini, F. Domenici, S.B. Dabagov, V. Guglielmotti, D. Hampai, L. Micheli, M. Titubante, C. Mazzuca, G. Paradossi, A. Palleschi, Ultrasound stimulated PVA-Microbubbles for Adhesive Removal from Cellulose-based Materials: A Groundbreaking Low Impact Methodology, *ACS Applied Materials & Interfaces* **13** (2021) 24207-24217 doi: 10.1021/acsami.1c01892
4. G. Baccolo, B. Delmonte, E. Di Stefano, G. Cibin, I. Crotti, M. Frezzotti, D. Hampai, Y. Iizuka, A. Marcelli and V. Maggi, Deep ice as a geochemical reactor: Insights from iron speciation and mineralogy of dust in the Talos Dome ice core (East Antarctica), *Cryosphere* **15**(10) (2021) 4807-4822.
5. N. Atanov,... D. Hampai et al, Final Design and Current Status of the Mu2e Crystal Calorimeter, *Proceedings of Science* **390** (2021) 759.
6. T. Albahri,. . . , S. Dabagov, D. Hampai et al, Measurement of the Anomalous Precession Frequency of the Muon in the Fermilab Muon g-2 Experiment, *Physical Review* **D103** (2021) 072002 doi: 10.1103/PhysRevD.103.072002
7. B. Abi,. . . , S. Dabagov, D. Hampai et al, Measurement of the Positive Muon Anomalous Magnetic Moment to 0.46 ppm, *Physical Review Letters* **126** (2021) 141801 doi: 10.1103/PhysRevLett.126.141801
8. T. Albahri,. . . , S. Dabagov, D. Hampai et al, Beam Dynamics Corrections to the Run-1 Measurement of the Muon Anomalous Magnetic Moment at Fermilab, *Physical Review Accelerators and Beams* **24** (2021) 044002 doi: 10.1103/PhysRevAccelBeams.24.044002
9. T. Albahri,. . . , S. Dabagov, D. Hampai et al, Magnetic-Field Measurement and Analysis for the Muon g-2 Experiment at Fermilab, *Physical Review* **A103** (2021) 042208 doi: 10.1103/PhysRevA.103.042208
10. S.B. Dabagov, A.V. Dik, Surface Channeling of Charged and Neutral Beams in Capillary Guides (Invited Review), *Quantum Beam Science* **6**(1) (2022) 8 doi: 10.3390/qubs6010008 (on volume cover)
11. M.I. Mazuritskiy, A.M. Lerer, A. Marcelli, S.B. Dabagov, Synchrotron Radiation Transmission by Two Coupled Flat Microchannel Plates: New Opportunities to Control the Focal Spot Characteristics, *Journal of Synchrotron Radiation* **29** (2022) 355-362 doi: 10.1107/S1600577521012893
12. K.B. Korotchenko, Y.P. Kunashenko, S.B. Dabagov, On Angular Features of Axial Channeling Radiation in Crystals, *Eur. Phys. J.* **C82** (2022) 196 doi: 10.1140/epjc/s10052-022-10147-w
13. 22. S.B. Dabagov, A.V. Dik, On Channeling of Charged Particles in a Single Dielectric Capillary, (2021) *arXiv:2109.03524 [physics.acc-ph]*

14. L.Sh. Grigoryan, A.H. Mkrtchyan, W.S. Wagner, S.B. Dabagov, A.A. Saharian, H.F. Khachatryan, V.R. Kocharyan, S.R. Arzumanyan, M.L. Grigoryan, V.Kh. Kotanjyan, H.P. Harutyunyan, Angular Distribution of High Power Radiation from a Chain of Charged Particles Rotating Around a Dielectric Ball, *Proc. Int. Conf. on Electron, Positron, Neutron and X-Ray Scattering under the External Influences* (Yerevan-Meghri, Oct. 18-24, 2021), Part 1, Publ. IAPP-Yerevan (2021) 27-35 ISBN 978-9939-1-1388-3
15. M.I. Mazuritskiy, A.M. Lerer, S.B. Dabagov, A. Marcelli, Coherent X-ray Fluorescent Excitation Inside MCP Microchannels: Axial Channeling and Wave Propagation, *Journal of Surface Investigation: X-ray, Synchrotron and Neutron Technique* **15**(3) (2021) 513-519 doi: 10.1134/S1027451021010286
16. M. Mazuritskiy, A. Marcelli, A. Lerer, S. Dabagov, M. Coreno, A. D'Elia, J. Rezvani, Wave Propagation and Focusing of Soft X Rays by Spherical Bent Microchannel Plates, *Journal of Synchrotron Radiation* **28** (2021) 383-391 doi: 10.1107/ S1600577520016458